IMPROVING PREDICTIONS OF GEOGRID-REINFORCED STONE COLUMN BEARING CAPABILITY: A COMPARATIVE ANALYSIS OF RES AND REGRESSION METHODS

H. Fattahi[*, †] and H. Ghaedi
Faculty of Earth Sciences Engineering, Arak University of Technology, Arak, Iran

ABSTRACT

Predicting the bearing capability (q_{rs}) of geogrid-reinforced stone columns poses a significant challenge due to variations in soil and rock parameters across different locations. The behavior of soil and rock in one region cannot be generalized to other regions. Therefore, accurately predicting q_{rs} requires a complex and stable nonlinear equation that accounts for the complexity of rock engineering problems. This paper utilizes the Rock Engineering System (RES) method to address this issue and construct a predictive model. To develop the model, experimental data consisting of 219 data points from various locations were utilized. The input parameters considered in the model included the ratio between geogrid reinforced layers diameter and footing diameter (d/D), the ratio of stone column length to diameter (L/dsc), the q_{rs} of unreinforced soft clay (qu), the thickness ratio of Geosynthetic Reinforced Stone Column (GRSB) and USB to base diameter (t/D), and the settlement ratio to footing diameter (s/D). Following the implementation of the RES-based method, a comparison was made with other models, namely linear, power, exponential, polynomial, and multiple logarithmic regression methods. Statistical indicators such as root mean square error (RMSE), mean square error (MSE), and coefficient of determination (R2) were employed to assess the accuracy of the models. The results of this study demonstrated that the RES-based method outperforms other regression methods in terms of accuracy and efficiency.

Keywords: Rock engineering system, regression methods, geogrid-reinforced stone columns, bearing capability, accuracy and efficiency.

---
[*]Corresponding author: Faculty of Earth Sciences Engineering, Arak University of Technology, Arak, Iran
[†]E-mail address: h.fattahi@arakut.ac.ir (H. Fattahia)

1. INTRODUCTION

Soft and very soft soil deposits pose significant challenges for geotechnical engineers and are subjects of extensive research and investigation. These soils are widespread in various regions, including major cities, and building structures on such soils often leads to high settlements and low shear strength. To address these issues, there is a strong need to enhance the resistance parameters of these soils. One effective method for improving the q_{rs} of soft soils is the utilization of stone columns. Stone columns increase the load-bearing capacity, reduce settlements, facilitate drainage, and mitigate excess pore water pressure. Additionally, this method is environmentally friendly as it does not require reinforcement or cement that could potentially harm the environment [1,2]. Early research on stone columns, conducted by researchers such as [3,4], highlighted their positive impact on load capacity increase and settlement reduction. Stone columns are primarily designed for soft soils and rely heavily on lateral confining pressure for their bearing capacity. Stability is achieved through the pressure exerted by the surrounding soil on the stone column. The concept of utilizing geosynthetic sheaths to enhance the q_{rs} of stone columns was introduced by Van Impe [5]. By enclosing the stone column with geotextile, the lateral pressure increases, preventing the granular materials of the stone column from settling into the soft soil and significantly enhancing the bearing capacity. If the shear strength of the soil surrounding the stone column is less than 15 kPa, a reinforced stone column is recommended over a standard stone column. To investigate the effects of geogrid reinforcement on the q_{rs} of soft clays, a series of laboratory tests were conducted, confirming that geogrid cylindrical reinforcements substantially increase the bearing capacity. When geogrid is used, the final q_{rs} of a stone column is 2 to 3 times higher compared to a case without a stone column [6,7].

Over the past three decades, numerous publications have focused on the qrsof geogrid-reinforced stone columns, with scholars conducting various investigations to gain a deeper understanding of the behavior of ground with stone columns. Some studies have employed numerical methods to analyze the qrsof geogrid-reinforced stone columns [8-12]. Others have utilized experimental and laboratory approaches to predict the q_{rs} of stone columns [13,14,8,15,16]. While these studies have provided valuable insights, the uncertainty and complexity of geological and geotechnical parameters in rock engineering cannot be fully addressed by experimental and numerical methods alone. Deterministic approaches that solely consider the behavior of soil and rock often yield low accuracy. Although laboratory methods exhibit better accuracy compared to experimental and numerical methods, they are time-consuming and costly. To overcome these limitations, modern technology and soft computing methods are now employed to construct complex nonlinear models that account for uncertainty.

The main focus of this paper revolves around the utilization of the RES-based method. This method, known for its simplicity and efficiency, proves to be highly practical and powerful in addressing rock engineering problems. It offers the capability to analyze multiple variables simultaneously that influence the q_{rs} of geogrid-reinforced stone columns. Additionally, the RES method takes uncertainties into account, enabling the construction of highly accurate models [17-19]. Consequently, extensive research utilizing the RES method has been conducted across various engineering disciplines, particularly in rock mechanics and mining. Examples include the assessment of vulnerability and risk following the Songun

copper mine explosion [20], quantitative analysis of gas and explosion risks in coal mines [21], estimation and prediction of penetration rates for TBM drilling machines in underground spaces [22], determination of rock mass deformation modulus [19], forecasting fragmentation and rock throwing hazards resulting from explosions in the Sarcheshme copper mine [23], prediction of fire risks in coal mine layers [24], fragmentation and explosion estimates for mines in Chile and Canada [25], the approach of rock mass injection to improve conditions in foundations, dams, and underground spaces [26], preparation of maps for estimating landslides in Sallekular located in the Jama river gorge [27], and evaluation of hazards associated with a pile shaft lodged in rock [18].

To address the uncertainties in the input parameters, a total of 219 data points obtained from various locations were considered. This research focuses on five key parameters that significantly impact the q_{rs} of geogrid-reinforced stone columns. The performance of the RES method was evaluated by employing statistical indicators such as mean square error (MSE), root mean square error (RMSE), and coefficient of determination (R2) to assess the accuracy of the obtained nonlinear and complex model. Furthermore, multiple regression methods were applied to the same input parameters and data to conduct a comparative analysis.

2. MODEL DATASET

In this research, a total of 219 data points were collected as experimental results. The following input parameters were considered: the ratio between geogrid reinforced layers diameter and footings diameter (d/D), the ratio of the stone columns length to diameter (L/dsc), the unreinforced soft clay bearing capacity (qu), the GRSB and USB thickness ratio to base diameter ratio (t/D), and the ratio of settlement to footing diameter (s/D). The q_{rs} of geogrid-reinforced stone columns was taken as the output parameter. Table 1 presents a partial overview of the input and output data [28].

Table 1. Partial input and output data for modeling [28]

Number	Inputs					Output
	d/D	L/d$_{sc}$	q$_u$(KPa)	t/D	s/D (%)	q$_{rs}$ (KPa)
1	0.00	6.00	7.09	0.00	0.84	11.39
2	0.00	6.00	15.56	0.00	1.72	23.10
3	0.00	6.00	23.26	0.00	2.60	33.81
4	0.00	6.00	30.77	0.00	3.65	44.57
5	0.00	6.00	37.28	0.00	4.98	53.39
6	0.00	6.00	41.84	0.00	6.41	60.63
7	0.00	6.00	45.35	0.00	8.24	66.70
8	0.00	6.00	47.86	0.00	10.22	73.48
9	0.00	6.00	49.83	0.00	12.21	78.46
10	0.00	6.00	51.36	0.00	14.20	83.56

Furthermore, Table 2 provides statistical descriptions of the model's input and output data, including minimum, maximum, average, standard deviation, and range values.

Table 2. Statistics description of inputs and output data set

Statistical index	d/D	L/d$_{sc}$	q$_u$ (kPa)	t/D	s/D (%)	q$_{rs}$ (kPa)
Minimum	0.000	2.000	4.210	0.000	0.500	11.390
Maximum	4.000	8.000	53.820	0.500	20.000	309.760
Mean	1.596	5.817	38.198	0.216	38.198	133.005
Standard deviation	1.562	1.085	15.723	0.114	6.420	77.352
Range	4.000	6000	49.610	0.500	19.500	298.370

Figure 1 displays the correlation scatter matrix between the input and output data. Negative correlation indicates an inverse relationship, while positive correlation signifies a direct relationship between the output and input data.
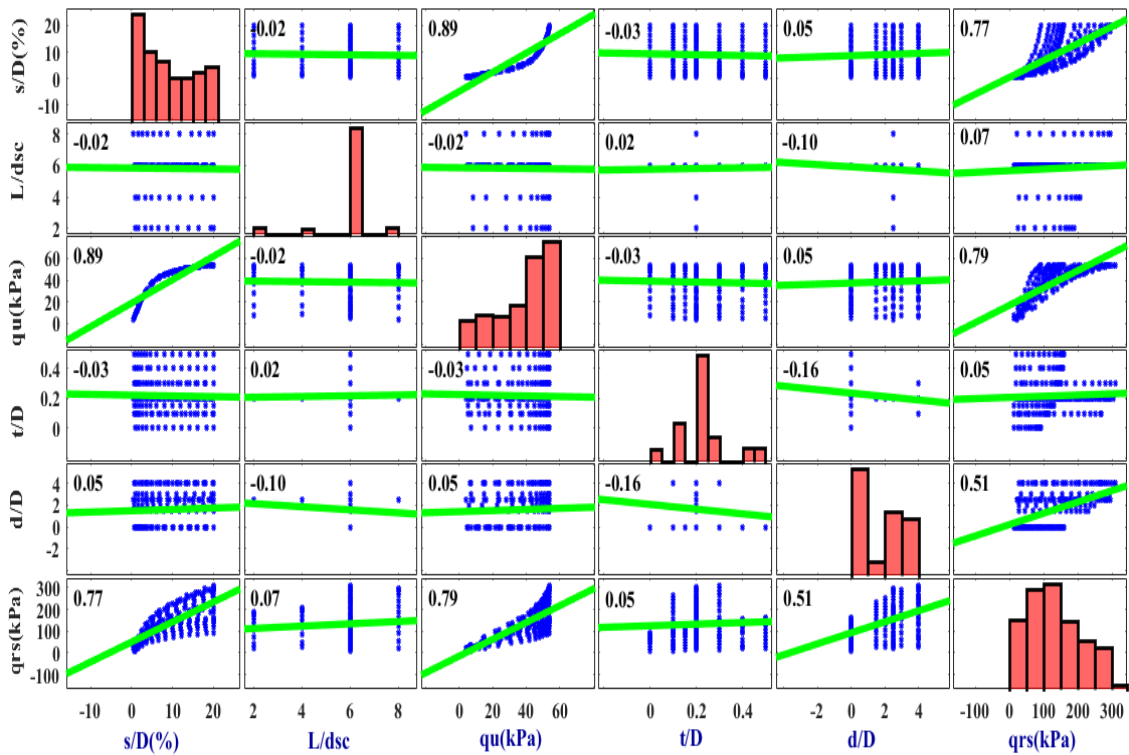

Figure 1. Correlation scatter matrix for cumulative distributions and statistical analyses

3. EXPERIMENTAL TECHNIQUE

3.1 Material Used

The experimental investigation involved the use of stone aggregate, geogrid materials, sand, and clay. Figure 2 showcases the gradation curves for the sand, stone, and clay aggregates. Clay served as the foundation bed for constructing the stone columns, while sand acted as the covering over the soft clay reinforced by stone columns. The clay's plasticity index, liquid limit, and plastic limit were measured and found to be 21%, 22%, and 43%,

respectively [28,29]. The soil is classified as inorganic clay with limited flexibility (CL) according to the System of Unified Soil Classification [30].
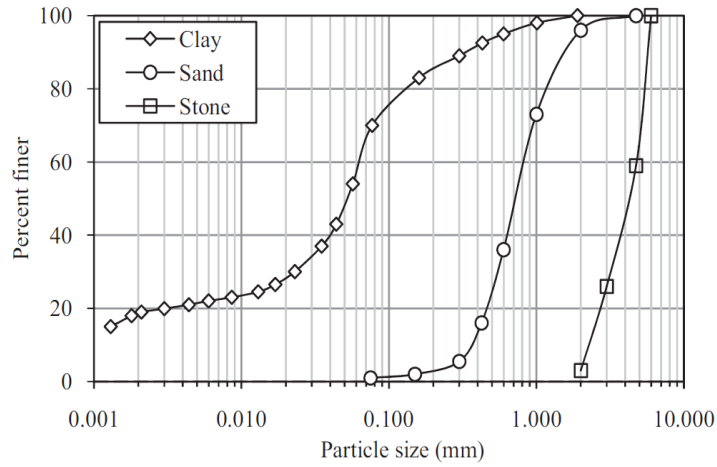

Figure 2. Particle size distribution curves for stone aggregate, sand and clay [28]

A series of undrained triaxial compression (UCS) tests were conducted on soil samples with varying water contents to determine the undrained shear strength (c_u) at a specific consistency. Figure 3 illustrates the variation of c_u with water content. The average water content for the soft clay throughout the experiments was approximately 32%. Based on calculations, the bulk density (γ) at this water content was determined to be 18.15 kN/m^3. A water content of 32% was selected based on the computed cu of 10 kPa.
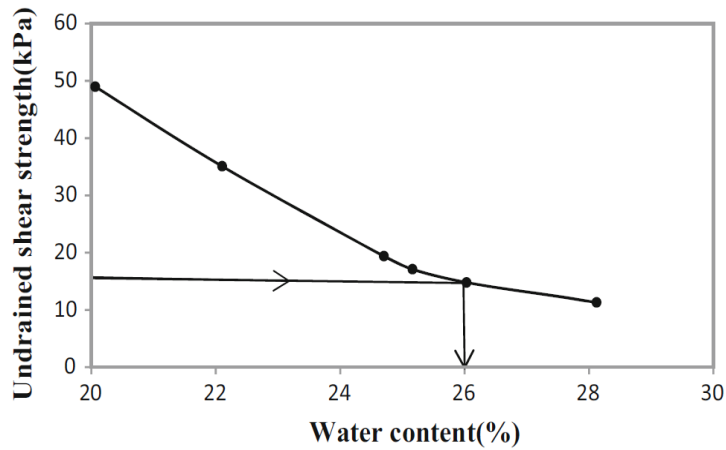

Figure 3. Variation of clay's undrained shear strength with water content [28]

Ill-graded crushed stone aggregates, ranging from 2 to 6 mm in particle size and exhibiting a coefficient of homogeneity of 2.13, were employed in the construction of the stone columns. These crushed stone aggregates demonstrate a compression density of 70%.

It was discovered that the bulk density of stone aggregate with a 70% relative density is 15.8 kN/m^3, and the angle of direct shear friction is 46°. Sand that passed through a 4.75 mm sieve to create the sand blanket, also known as the sand bed, had uniformity and curvature factors of 3.4 and 0.7, respectively. The relative density of the sand bed was 70% across all of the experiments. The shear strength values for sand samples with a relative density of 70% in the triaxial CD test were cohesion 0 and internal friction angle 42°; the bulk density at a relative density of 70% was 16.7 kN/m^3. The sand bed was reinforced with a biaxial geogrid layer constructed of high-density polyethylene. According to ASTM D6637 [29], Table 3 lists the characteristics of the geogrid reinforcement.

Table 3. Geogrid properties

Parameter	Value
Strain with maximum force (%)	16
Thickness (mm)	1.5
Mesh aperture size (mm×mm)	10×10
Strength at ultimate tension (kN/m)	20
Shear stiffness at ultimate strain [J (kN/m)]	125
Mass (g/m^2)	190

3.2 Test setup

The test setup involved using a square tank with dimensions of 1000 mm length, 1000 mm width, and 1000 mm height, as shown in Figure 4. Initially, a single thick polythene sheet was applied to the inside walls of the test tank to reduce friction and prevent water loss. Layers of 100 mm thick soft clay were then added to the tank to create the desired thickness. The density and water content of the clay remained constant throughout all the testing. To achieve a bulk density of 18.15 kN/m3, the required weight of dry clay for a 100 mm thickness was mixed with 32% water. Steel rammers of 50 mm and 120 mm were used to compact and crush the clay lump inside the tank. After the tank had been empty for seven days, a plastic cover was placed over the clay-filled tank. Undisturbed soil samples were collected from various areas of the test bed using thin-walled cylinder samplers, and their properties were evaluated. Additionally, vane shear experiments were conducted at several locations on a smaller scale. The clay in the test beds had a bulk unit weight of 18.15 kN/m3, shear strength of 10 kPa, and an average moisture content of 32%. The coefficient of variance ranged from 1.3%.

Each column in the group test was constructed using a clay substrate. A steel pipe with a 50 mm-deep open end and inner and outer diameters of 48.5 mm and 50 mm, respectively, was inserted into the clay bed at the desired position. Earth was removed using steel spiral augers and a steel pipe, with the auger drilling a 300 mm hole through the steel pipe while pushing it. The inner surface of the steel tube was coated with a thin layer of oil throughout the testing. The diameter of the spiral was slightly smaller than the inner diameter of the steel pipe. The helical augers penetrated the clay in increments of 50 mm to facilitate the removal of clay. The relative density of the stone columns in all test series was maintained at 70%. The weight of stone required was calculated based on the volume of the hole. Five identical pieces of stone, each weighing the calculated amount, were cut out and filled into

the hole, ensuring uniform compaction up to a height of 50 mm. Compaction was initially performed using a steel tamper with a 15 mm diameter, followed by one with a 25 mm diameter.
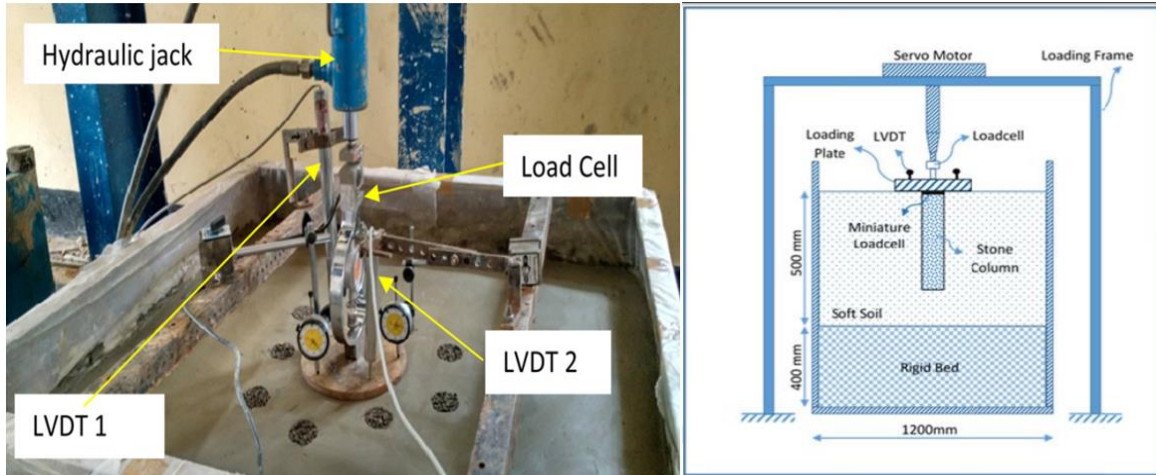

Figure 4. Illustration of the experimental setup [28]

Figure 5 illustrates the arrangement of the stone pillars. The three middle stone columns' performance can be observed in Figure 5. To simulate the field condition of compaction of the intervening soil, a 3-column group test should include at least 12 columns, following IS 15284 Part I [31].
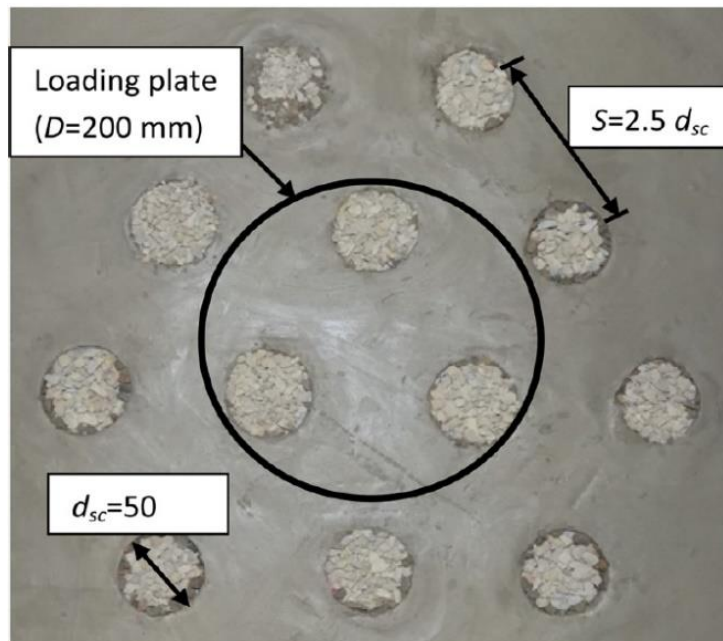

Figure 5. Plan view of a group of stone

The columns in this study were arranged in a triangular configuration with a spacing of

2.5 times the diameter of the column. Dry sand layers were compressed by a circular steel hammer, achieving specific gravity up to a relative density of 70%. In the case of a GRSB [32], a 5 mm layer of sand was added on top of the clay substrate. A geogrid was placed in a circular arrangement at the center of the stone column group, and the required thickness was achieved in the sand bed. The foundation consisted of a sturdy steel plate with a thickness of 15 mm and a diameter equal to the footing diameter (D). The footing was positioned in the middle of the tank for each test.

3.3 Test procedure

Each test involved applying a load to the foundation using a hydraulic jack and a load cell capable of supporting 100 kN. The load was increased incrementally, with equal quantities of load applied at each step, until the footing reached a state of stabilization settling where no noticeable change in settlement occurred (i.e., less than 0.02 mm/min). During each load increment, settlement was measured using two LVDTs positioned at diametrically opposed ends of the footing, with a minimum count of 0.01 mm. A 12-channel portable data acquisition device was used to record the data from the LVDTs and load cell. Before conducting the tests, all equipment was calibrated properly. The load in each test was applied until 20% of the footing diameter had completely settled. Additionally, a thin cement slurry was injected into the three central stone columns to analyze any bulging and lateral deformations that occurred following the load test, without disturbing the columns. Table 4 provides an overview of the tests conducted for this project.

Table 4. Summary of the experiment

Testing series	Reinforcement style	Specifics of the parameters examined
1	SC+Clay	L=300mm, d_{sc}=50mm, S=2.5×d_{sc}
2	USB+ SC+Clay	Variables: t/D= 0.3, 0.4, 0.5, 0.1, 0.15, 0.2 Constants: L/d_{sc}=6, S/d_{sc}=2.5
3	GRSB+SC+Clay	Variables: t/D=0.1, 0.3, 0.2 Constants: S/d_{sc}=2.5, d/D=4, L/d_{sc}=6
4	GRSB+ SC+Clay	Variables: d/D=2.5, 3.0, 1.5, 2.0 Constants: L/d_{sc}=6, S/d_{sc}=2.5, t/D=0.2
5	GRSB+ SC+Clay	Variables: L/d_{sc} =4.0, 8.0, 2.0 Constants: t/D=0.2, d/D=2.5, S/d_{sc}=2.5

4. STATISTICAL MODELING

4.1 Multiple Linear Regression Analysis (MLR)

In the field of rock engineering, multiple linear regression is commonly used to establish relationships and estimate models. This method involves finding a linear relationship between several independent variables (input parameters) and a dependent variable (output or prediction parameter). The equation for the multiple regression line is as follows:

$$y = B_0 + B_1 x_1 + B_2 x_2 + \ldots + B_n x_n + e \tag{1}$$

In the equation, y represents the dependent parameter, x denotes the independent parameters, e is the error term, and $B_0, B_1, B_2, \ldots B_n$ represent unknown regression coefficients that need to be determined. A higher dispersion and deviation around the regression line indicate a lower quality prediction model, while less divergence between the points on the regression line indicates a more accurate prediction. In this study, a linear multiple regression analysis was performed using the statistical program SPSS. The dependent variable q_{rs} was analyzed with the independent variables d/D, L/d$_{sc}$, q$_u$ (kPa), t/D and s/D (%). The resulting model with a carefully predicted R^2 value of 0.8752 is presented as follows:

$$q_{rs}(kPa) = -118.25 + 25.36\,d/D + 10.37\,L/d_{sc} + 7.304 q_u(kPa) + 107.68\,t/D + 4.264\,s/D\,(\%) \tag{2}$$

To evaluate multicollinearity, the study examined significant correlations between independent variables. Multicollinearity occurs when independent variables provide redundant information, leading to inaccurate conclusions. The variance inflation factor (VIF) is commonly used to assess the extent of linear relation. Table 5 provides computed VIF values for the independent variables. If the obtained VIF is greater than 10, it may cause issues for the multiple linear relationship [33,34].

Table 5. Collinearity and MLR coefficients for Eq. (2)

Independent variables	Unstandardized coefficients		Standardized coefficients β	95.0% Confidence interval for B		Collinearity statistics		t values	R^2	Standard error of estimate
	B	Std.error		Lower bound	Upper bound	Tolerance	VIF			
Constant	-118.246	13.476		-144.850	-92.643			-8.774		
d/D	25.361	1.183	0.526	23.025	27.697	0.943	1.060	21.431		
L/dsc	10.373	1.932	0.129	-14.188	-6.559	0.991	1.009	5.368	0.951	24.691
qu(kPa)	2.304	0.267	0.445	-2.830	-1.777	0.214	4.667	8.635		
t/D	107.681	15.667	0.168	76.754	138.60	0.951	1.051	6.873		
s/D(%)	4.264	0.631	0.349	-5.509	-3.019	0.214	4.667	6.762		

Table 6 presents the analysis of variance (ANOVA) and regression results for Eq. (2). The model's significance and the F (Sig.) value are utilized to determine whether the null hypothesis of "no effect" can be rejected. In this study, the obtained F value was 317.630, and the Sig. value was 0.000 (less than 0.05). These results indicate that the null hypothesis can be rejected, providing evidence of a significant effect.

Table 6. Variance analysis for Eq. (2)

	Sum of squares	df	Mean square	F	Sig.
Regression	968244.410	5	193648.882	317.630	0.000
Residual	103034.071	169	609.669		
Total	1071278.482	174			

4.2 Multivariate Regression Models

In addition to multiple linear regression analysis, various multivariate regression models, including power, exponential, polynomial, and logarithmic models, were investigated to estimate the qrsof geogrid-reinforced stone columns as the dependent variable. These models were applied using the same dataset as the multiple linear regression analysis. The mathematical formulas for each model and their corresponding R^2 values are provided below:

The power model (with $R^2=0.7794$), is:

$$q_{rs}(kPa) = 10^{(1.07+0.023d/D+0.081L/d_{sc}+0.01q_u(kPa)+0.00001t/D+0.003s/D(\%))} \tag{3}$$

The exponential model (with $R^2 = 0.7429$) is:

$$q_{rs}(kPa) = \exp(3.464+0.176d/D+0.71L/d_{sc}+0.0075q_u(kPa)+ \\ 0.777t/D+0.006s/D(\%)) \tag{4}$$

The polynomial model (with $R^2=0.8564$), is:

$$q_{rs}(kPa) = -32.356+2.827q_u(kPa)+0.165(s/D(\%))^2-29.584(t/D)^3 \\ +0.289(d/D)^4+0.002(L/d_{sc})^5 \tag{5}$$

The logarithmic model (with $R^2=0.9037$), is:

$$q_{rs}(kPa) = 196.312+161.861\ln(d/D+L/d_{sc}+t/D)-43.726\ln(q_u(kPa))+ \\ 86.758\ln(s/D(\%)) \tag{6}$$

5. ROCK ENGINEERING SYSTEMS (RES)

Designing rock engineering projects for mining or construction purposes requires consideration of all relevant variables and understanding their mutual effects within a system. To facilitate this process, the rock engineering systems method was developed by Hudson in 1992 as a tool for investigating the interplay of factors in a system. This approach becomes necessary when dealing with highly complex issues that cannot be solved using conventional methods alone [35]. In the RES approach, an interaction matrix is utilized to examine the effects of all interactions. As depicted in Figure 6, the main factors or input parameters are placed along the main diagonal of the matrix, while the interactions between these factors are represented in other elements. These interactions are coded using specific numbers to determine and quantify their effects. By performing calculations on the columns and rows, the results can be obtained. In the matrix, the influence of parameters on each other follows a clockwise pattern, with the lower-left quadrant indicating the effect of parameter B on A, and the upper-right quadrant representing the effect of parameter A on B.
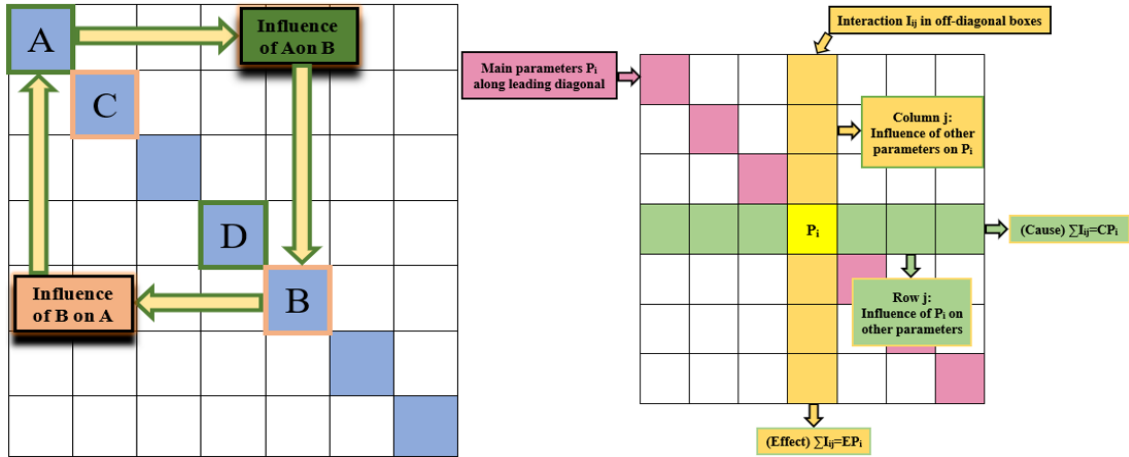
Figure 6. Concept of interaction matrix in RES [35]

To code the interaction matrix and represent the intensity of influence among parameters, several methods are commonly used, including the explicit method, probabilistic expert semi-quantitative (PESQ) method, continuous quantitative coding (CQC) [36], binary method, and expert semi-quantitative (ESQ) method [35]. Among these methods, the ESQ method is frequently employed due to its simplicity and high accuracy. Table 7 outlines the ESQ method, which involves assigning scores ranging from 0 to 4 to indicate the strength of interaction between two parameters. A score of 4 signifies a significant dependence and relationship according to experts and engineers.

Table 7. Expert semi-quantitative method [35]

Code number	Concept
0	No interaction
1	Low interaction
2	Moderate interaction
3	High interaction
4	Intense interaction

Upon completion of coding the interaction matrix, a cause-effect diagram can be constructed. In this diagram, the sum of each row represents the "cause" or the effect of a parameter on the system, while the sum of each column denotes the "effect" or the effect of the system on the parameter. Drawing the cause-effect diagram involves transferring the cause and effect values (C and E) onto a coordinate axis. The position of each point in the space (c and E) determines the interaction status of that parameter. The higher the numerical value of the sum of cause and effect values (C+E) for a factor, the stronger its interaction with the entire system. Additionally, the numerical value of the subtraction of cause and effect (C-E) indicates the degree of dominance of that factor on the system. The cause and effect values (C+E) aid in drawing the cause-effect diagram for each parameter. Using Equation (7) [37], the percentage value (C + E) can be used to derive the weight (ai) of parameter *i*:

$$a_i = \frac{(C_i + E_i)}{(\sum_{i=1}^{n} C_i + \sum_{i=1}^{n} E_i)} \times 100 \tag{7}$$

The vulnerability index (VI) is a metric proposed by Benardos, Kaliampakos [37] within the RES-based method to characterize the damage and collapse zones of underground tunnels excavated using TBM. The vulnerability index is calculated using Equation (8) [37].

$$VI = 100 - \sum_{i=1} a_i \frac{Q_i}{Q_{max}} \tag{8}$$

In Equation (8), a_i represents the weight of the ith parameter obtained from Eq. (7), Q_{max} is the maximum value (rating) of the parameters, and Q_i represents the value of each parameter. Table 8 provides the classification of the vulnerability index based on Eq. (8). Higher values indicate higher project risks, while lower values indicate lower risks. In this research, the vulnerability index has been utilized to create a model for predicting the qrsof geogrid-reinforced stone columns.

Table 8. Classification of the VI [37]

Risk description	Low-medium	Medium-high	High-very high
VI	0-33	33-66	66-100
Category	I	II	III

5.1 Multivariate Regression Models

Table 9 presents the essential parameters used to construct the q_{rs} model based on the RES method.

Table 9. Input parameters used for creating the res-based model

|	Parameter	Symbol
P_1	Ratio between geogrid reinforced layers diameter and footings diameter	d/D
P_2	Ratio of the stone columns length to diameter	L/d_{sc}
P_3	Unreinforced soft clay bearing capacity	q_u (kPa)
P_4	GRSB and USB thickness ratio to base diameter ratio	t/D
P_5	Ratio of settlement to footing diameter	s/D (%)

5.2 Multivariate Regression Models

The ESQ approach, pioneered by Hudson, serves as the basis for coding the interaction matrix [35]. By utilizing a questionnaire and gathering input from multiple experts and engineers, this approach determines how key factors will impact the model. In this study, based on the input from mining and geotechnical engineers, the interaction matrix consists of five key parameters that significantly influence the q_{rs} of geogrid-reinforced stone columns, as shown in Table 10.

Table 10. Effect of input parameters on q_{rs} in the interaction matrix

P_1	2	0	0	1
1	P_2	0	0	1
0	3	P_3	3	3
1	1	3	P_4	2
2	2	2	2	P_5

Figure 7 displays the cause-effect diagram for these five parameters. In this diagram, the main diameter represents the geometric location of C=E. Along this diameter, the sum of C+E values increases, and lines of equal interaction intensity are drawn on the graph to differentiate between high and low interactions. Points located in the lower right part of the diagram indicate parameters that dominate the system, as they have larger C-E values compared to points around the diameter. Parameters affected by the system are placed in the upper left part of the diagram and have smaller C+E values. The cause-effect diagram is crucial for understanding the role of each parameter in the project and identifying beneficial and non-beneficial interactions from an engineering perspective. By calculating the amount of interaction in terms of C+E values, parameters that require control can be identified, as changes in these parameters may induce significant changes in the system. Based on Figure 7, parameters 1 and 5, which represent the ratio between the diameter of reinforced geogrid layers and the diameter of the foundation, and the ratio of settlement to the diameter of the foundation, respectively, are greatly affected by the system. Additionally, parameter 4, which denotes the ratio of the thickness of GRSB and USB to the base diameter, has the most significant impact on the system. In the next step, as evident from Figure 8, parameter 1 (the ratio between the diameter of the geogrid reinforced layers and the diameter of the foundations) exhibits the highest intensity of interaction in the system compared to other parameters. A small change in this parameter can lead to substantial changes in the system.
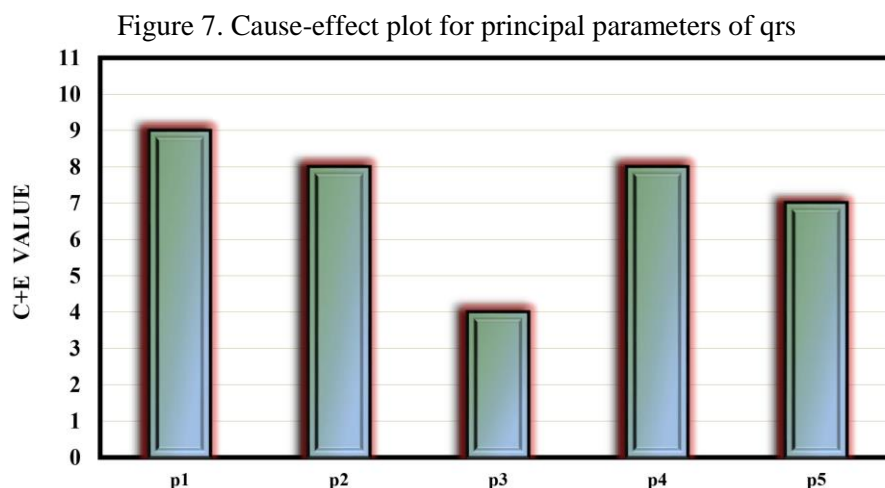
Figure 7. Cause-effect plot for principal parameters of qrs
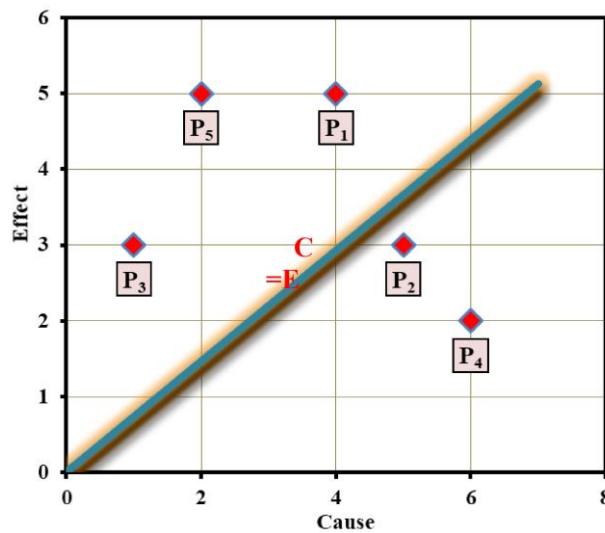
Figure 8. Cause+Effect values for principal parameters of qrs

5.3 Multivariate Regression Models

The values of the input parameters are ranked to determine the vulnerability index for each dataset. These parameters are typically divided into five categories ranging from 0 to 4, reflecting their effects on the q_{rs} of geogrid-reinforced stone columns. A rating of 0 in this classification represents the worst or most unfavorable state, while a rating of 4 indicates the best or most favorable state. Based on input from specialists in mining engineering, rock mechanics, and geotechnics, Table 11 suggests rating ranges for the elements determining qrs.

Table 11. Suggested ratings and ranges

Number	Parameters		Values and Ratings				
1	d/D	Value	0-0.09	0.09-1.6	1.6-2.2	2.2-3.5	>3.5
		Rating	0	1	2	3	4
2	L/d$_{sc}$	Value	<3	3-5	5-6.5	6.5-7.5	7.5>
		Rating	0	1	2	3	4
3	q$_u$ (kPa)	Value	0-15	15-25	25-35	35-50	>50
		Rating	0	1	2	3	4
4	t/D	Value	0-0.09	0.09-1.6	1.6-2.2	2.2-3.5	>3.5
		Rating	0	1	2	3	4
5	s/D (%)	Value	<3	3-5	5-13	13-16	>16
		Rating	0	1	2	3	4

5.4 Multivariate Regression Models

In order to predict the q_{rs} of stone columns reinforced with geogrid, a dataset comprising 219 data points was utilized. Out of these, 176 data points, equivalent to 80% of the data, were utilized for model training and construction, while the remaining 43 data points (20% of the data) were used for evaluating the accuracy of the model. To provide further clarity, an example calculation of the vulnerability index for dataset number 1 is presented in Table

12.

Table 12 Values, Ratings, and Vulnerability Indices for Dataset Number 1.

Parameters	d/D	L/d_{sc}	q_u (kPa)	t/D	s/D (%)
Value or description	0	6	7.09	0	0.84
Value rating (Qi)	0	2	0	0	0
Weighting (% ai)	25	22.2	11.11	22.2	19.44
VI	90.27				

Furthermore, Figure 9 illustrates the variations in the vulnerability index (VI) for the 176 data points. The average VI, which is calculated as 16.36, indicates the presence of the third group of risks (low to medium).
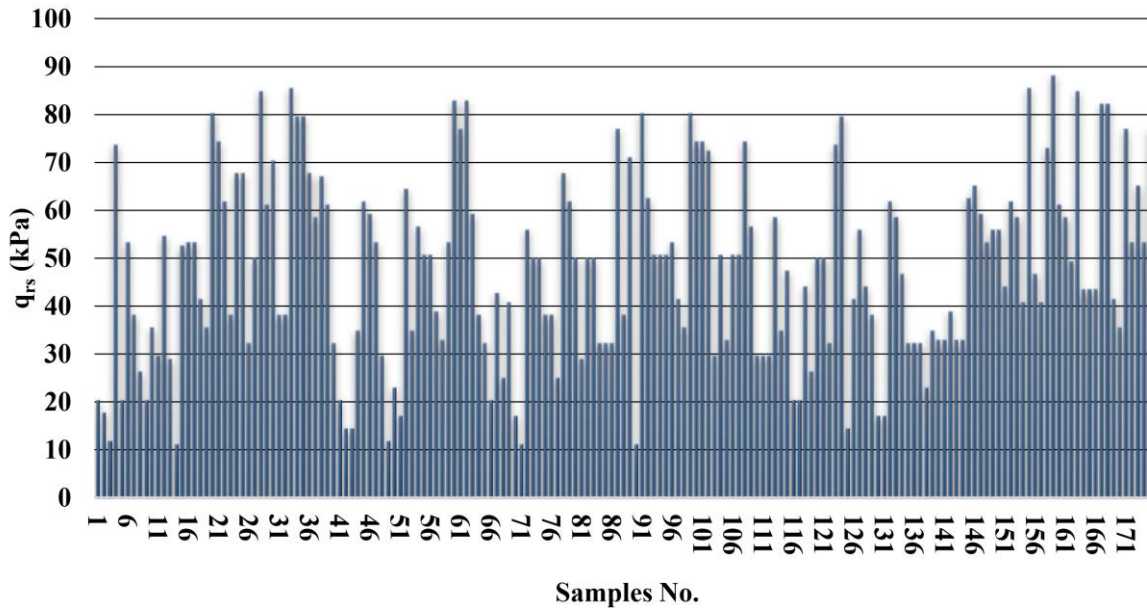

Figure 9. VI for the Sample Data Points

After calculating the vulnerability index for the entire dataset of 219 data points, a regression analysis based on the RES method was conducted. As shown in Figure 10, a polynomial regression analysis was performed using 176 data points, resulting in a coefficient of determination of 0.8914. Considering the high accuracy of the developed equation (Eq. (8)) during the training phase, it can be concluded that the built model can effectively predict the q_{rs} of stone columns reinforced with geogrid.

$$q_{rs} = 0.0309VI^2 - 6.7729VI + 378.55 \tag{9}$$

H. Fattahia and H. Ghaedi
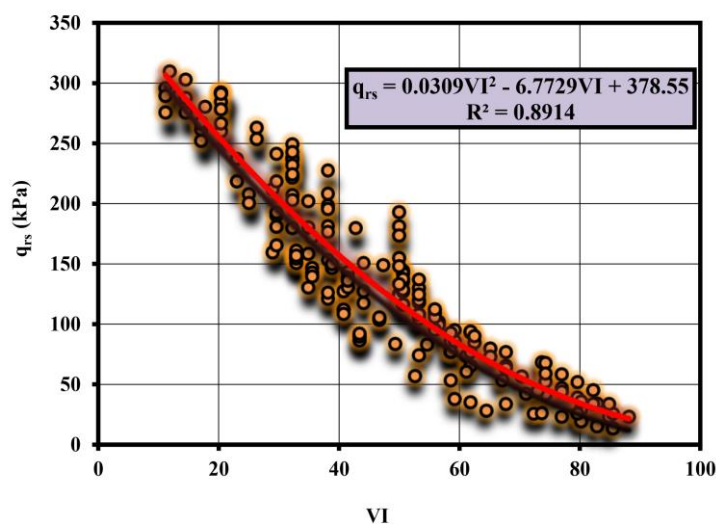
Figure 10. qrs–VI prediction model

6. RESULTS AND EVALUATION OF MODEL PERFORMANCE

After constructing the models using 176 data points, the remaining 43 data points were used to evaluate the built model. Table 13 presents a comparison of the predicted values for the 43 data points based on linear, power, exponential, polynomial, logarithmic, and RES-based equations.

Table 13. Comparison of Obtained Values from the Built Models and Measured q_{rs} of Geogrid-Reinforced Stone Columns

VI	Measured q_{rs}	Predicted q_{rs}					
		Linear	Power	Exponential	Polynomial	Logarithmic	RES
90.78	11.39	2.94	36.77	51.84	3.35	10.06	9.26
61.18	66.7	45.37	42.27	72.20	122.60	76.52	73.711
61.18	78.46	68.84	43.89	76.47	148.66	139.88	79.82
88.15	11.5	5.73	36.59	55.30	6.55	14.28	12.79
58.55	99.49	79.88	43.91	82.70	148.94	108.69	87.91
64.47	67.52	29.09	40.48	71.68	90.88	44.28	70.32
40.78	115.06	118.66	46.75	89.24	201.31	147.15	145.53
28.94	188.56	142.84	170.20	147.68	175.08	157.75	208.38
28.94	238.83	171.08	200.94	158.62	205.71	195.40	219.96
55.92	85.48	45.49	95.90	77.37	104.39	59.30	96.43
55.92	97.38	59.37	106.75	80.67	120.24	77.42	96.43
38.15	129.31	124.04	142.62	128.13	201.24	148.47	157.46
82.89	29.73	52.44	46.93	62.59	14.79	12.84	29.44
53.28	98.32	50.39	95.51	80.31	103.68	92.35	105.37
82.89	18.23	16.25	39.23	64.39	11.40	21.57	21.15

Three statistical indices, MSE, RMSE, and R^2, were used to assess the accuracy of the developed models. In this evaluation, a smaller value of MSE and RMSE and a larger value

of R2 indicate that the predicted values of the q_{rs} of geogrid-reinforced stone columns are closer to the actual measurements, signifying higher accuracy of the built model [38-41]. The equations for these criteria are as follows:

$$\text{MSE} = \frac{1}{n}\sum_{k=1}^{n}\left(t_k - \widehat{t_k}\right)^2 \tag{10}$$

$$\text{RMSE} = \sqrt{\frac{1}{n}\sum_{k=1}^{n}\left(t_k - \widehat{t_k}\right)^2} \tag{11}$$

$$R^2 = 1 - \frac{\sum_{k=1}^{n}\left(t_k - \widehat{t_k}\right)^2}{\sum_{k=1}^{n}t_k^2 \dfrac{\sum_{i=1}^{n}\widehat{t}^2}{n}} \tag{12}$$

In the above equations, n represents the number of samples, t_k represents the real amount, and $\hat{t}_n$ represents the predicted value for the kth observation [42-44]. Table 14 presents the analysis of the models created for the 43 data points using power regression, linear regression, exponential regression, logarithmic regression, polynomial regression and RES regression. The results in the table demonstrate that the RES-based model exhibits higher accuracy compared to other methods, with MSE = 0.0038, RMSE = 0.0620, and R^2 = 0.9552 for predicting the q_{rs} of geogrid-reinforced stone columns.

Table 14. Performance Results of Different Constructed Models

Models	MSE	RMSE	R^2	Observations
Linear	0.0101	0.1008	0.8752	43
Power	0.0215	0.1466	0.7794	43
Exponential	0.0395	0.1988	0.7429	43
Polynomial	0.0140	0.1186	0.8564	43
Logarithmic	0.0082	0.0909	0.9037	43
RES	0.0038	0.0620	0.9552	43

To further assess the evaluation of the built models, Figure 11 displays a spider diagram depicting the accuracy of the models using the statistical parameters MSE and R^2 for different models.
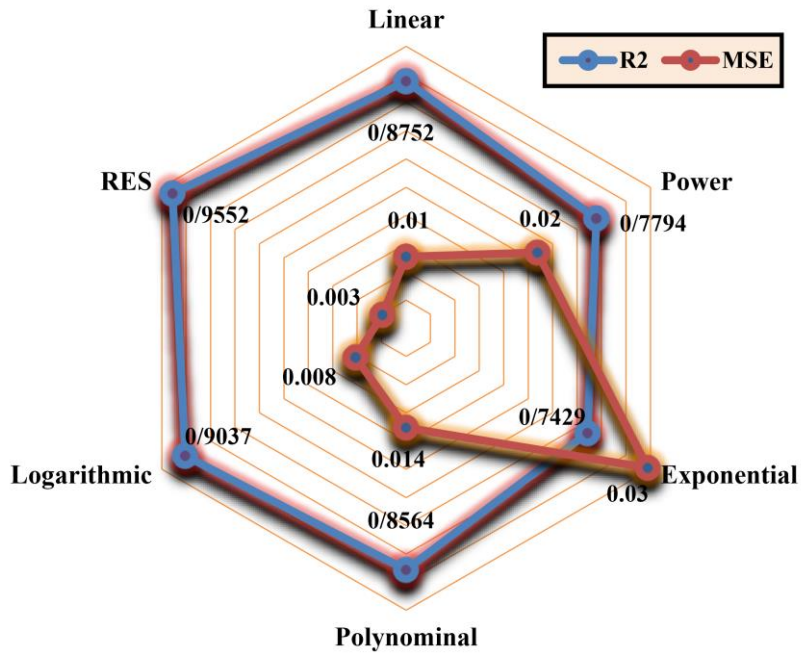
Figure 11. Comparing the Results and Evaluating the Performance of the Statistical Parameters
MSE and R2 for All Types of Built Models

To facilitate a comparison between the values obtained from the models constructed in
Table 13, Figure 12 illustrates the comparison between the RES-based model and other
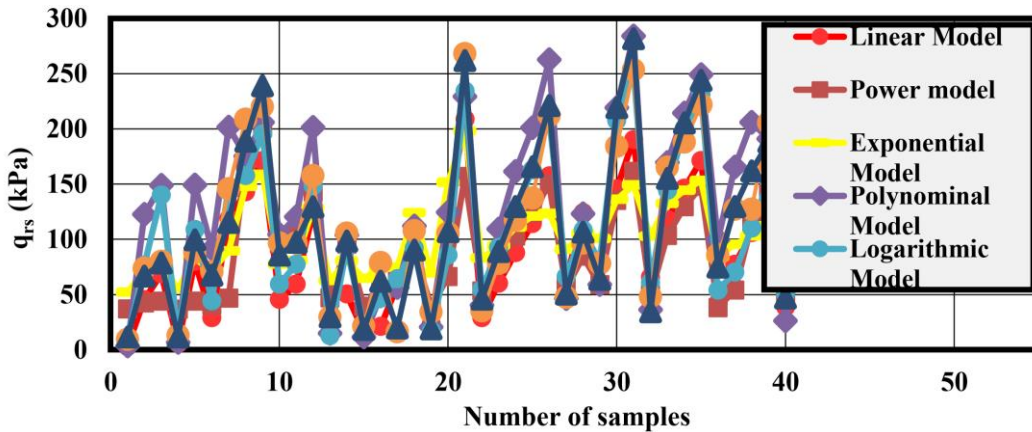regression methods for the 43 data points.

Figure 12. Comparison of Measured and Predicted q_{rs} using Polynomial Model, Exponential
Model, Logarithmic Model, Power Model, and RES-based Mod

Based on the findings of this study, it can be concluded that the RES-based method
exhibits higher accuracy compared to other regression methods due to the close proximity of
the actual values to the predicted values. Hence, as depicted in Figure 13, the relationship
established using the RES method aligns well with the actual values, and the developed

model can be utilized with high accuracy to predict the q_{rs} of geogrid-reinforced stone columns.
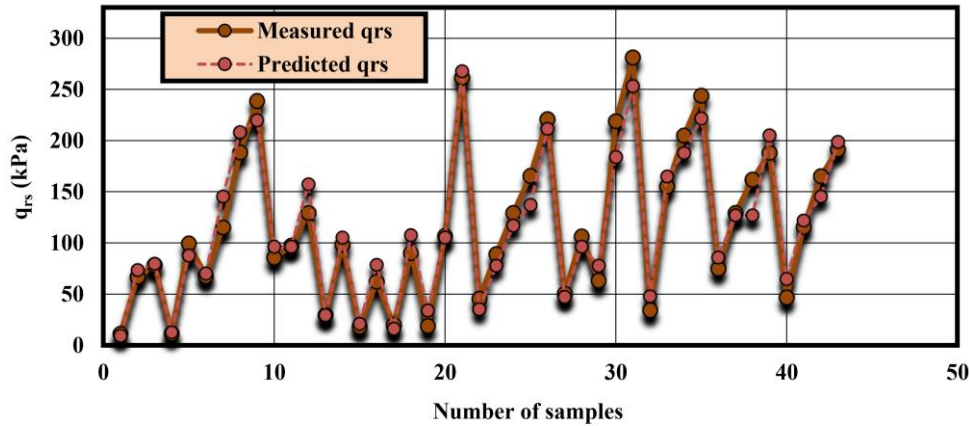

Figure 13. Comparison of Measured and Predicted q_{rs} for the RES-based Model

7. CONCLUSION

The construction of stone columns has proven to be an effective, cost-efficient, and environmentally friendly method for improving cohesive and loose soils. This method has been utilized for years to address settlement issues, enhance bearing capacity, reduce liquefaction potential, and expedite the consolidation process of loose soils. Given the significance and widespread application of stone columns in mitigating various geotechnical problems, it becomes crucial to accurately estimate the q_{rs} of geogrid-reinforced stone columns. However, the values of soil and rock parameters vary at different locations, leading to uncertainties in the project. Therefore, minimizing uncertainties and achieving accurate estimations are vital for reliable predictions of stone column behavior.

To address this challenge, a new RES-based method was developed in this study to enhance the prediction of geogrid-reinforced stone column bearing capacity in mining and geotechnical applications. The RES technique takes into account the nonlinearity and complexity of soil and rock behavior, as well as the influence of crucial parameters on the q_{rs} of geogrid-reinforced stone columns. By constructing a comprehensive and nonlinear model, the RES technique enables more accurate and reliable predictions of stone column behavior.

To assess the effectiveness of the RES-based approach, an experimental dataset comprising 219 data points obtained from various locations was utilized. Five input parameters, namely d/D, L/dsc, qu (kPa), t/D, and s/D (%), were considered as influential factors in estimating qrs. The findings of this study demonstrated that the RES-based method outperformed other regression methods in estimating the q_{rs} of geogrid-reinforced stone columns, with performance metrics of MSE=0.0038, RMSE=0.0620, and R^2=0.9552.

These results highlight the success of the RES-based method in overcoming the limitations of conventional approaches and improving the accuracy of predicting q_{rs} of geogrid-reinforced stone column. The RES technique provides a powerful tool for

geotechnical engineers and rock mechanics specialists to address soil and rock behavior challenges by considering uncertainties, avoiding simplifications, and accounting for the influence of critical parameters. The implications of this research are significant for engineers and researchers involved in mining and geotechnical projects. Accurate prediction of q_{rs} of geogrid-reinforced stone column enables optimized design, enhanced safety measures, mitigation of potential failures, and increased overall productivity in stone and mining projects. The RES-based approach empowers engineers to make well-informed decisions regarding stone column design and construction by providing valuable insights and assistance in the decision-making process.

In conclusion, the utilization of the RES method presented in this study offers a robust tool for enhancing the accuracy of predicting q_{rs} of geogrid-reinforced stone column in mining and geotechnical projects. The research results underscore the potential of the RES method to revolutionize the fields of geotechnical engineering and rock mechanics by enabling engineers to overcome challenges and optimize stone column-based structures for improved safety and efficiency in mining and geotechnical operations.

REFERENCES

1. Mohapatra SR, Rajagopal K, Sharma, J Direct. shear tests on geosynthetic-encased granular columns. *Geotext Geomem,* 2016; **44**(3), 396-405
2. Castro J: Groups of encased stone columns: Influence of column length and arrangement. *Geotextiles and Geomembranes* 2017; **45**(2), 68-80
3. Greenwood D. Mechanical improvement of soils below ground surface. In: Inst Civil Engineers Proc, London/UK/ 1970
4. Hugher J, Withers N: Reinforcing of soft cohesive soils with stone columns. *Ground engineering* 1974; **7**(3)
5. Van Impe WF. *Soil improvement techniques and their evolution.* (1989)
6. Murugesan S, Rajagopal K. Geosynthetic-encased stone columns: numerical evaluation. *Geotext Geomem,* 2006; **24**(6), 349-358
7. Nazari Afshar J, Ghazavi M. A simple analytical method for calculation of bearing capacity of stone-column. *Int J Civil Eng,* 2014; **12**(1), 15-25
8. Xu F, Moayedi H, Foong LK, Moghadam MJ, Zangeneh M. Laboratory and numerical analysis of geogrid encased stone columns. *Measurement* 2021; **169**, 108369
9. Pandey B, Rajesh S, Chandra, S. Numerical Analysis of Soft Soil Reinforced with Geogrid Encased Stone Column. *In: Proceedings of the 7th Indian Young Geotechnical Engineers Conference: 7IYGEC-2019 2022*, pp. 65-72. Springer
10. Tan X, Hu Z, Chen C, Zhao M. 3D DEM-FDM coupled analysis of the behavior of an isolated geogrid-encased stone column under axial loading. *J Geotech Geoenv Eng,* 2021; **147**(6), 04021028
11. Jala SK, Sharma S, Bhat AH. Effect of Sand Blanket Reinforced with Geogrid Over the Stone Column in Compressible Clay Soils: 3D Numerical Study. *In: Proceedings of Indian Geotechnical and Geoenvironmental Engineering Conference (IGGEC) 2021, Vol. 1 2022*, pp. 397-406. Springer

12. Dural SB, Ertugrul ÖL. Numerical analysis of the geosynthetic reinforced stone columns with Plaxis2D finite element code. *Adv Eng Days, (AED)* 2022; **5**, 165-167

13. Mehrannia N, Nazariafshar J, Kalantary F. Experimental investigation on the bearing capacity of stone columns with granular blankets. *Geotech Geolog Eng,* 2018; **36**, 209-222

14. Hataf N, Nabipour N, Sadr A. Experimental and numerical study on the bearing capacity of encased stone columns. *Int J Geo-Eng,* 2020; **11**, 1-19

15. Dash SK, Bora MC. Influence of geosynthetic encasement on the performance of stone columns floating in soft clay. *Canadian Geotech J,* 2013; **50**(7), 754-765

16. Miranda M, Da Costa A, Castro J, Sagaseta C. Influence of geotextile encasement on the behaviour of stone columns: Laboratory study. *Geotext Geomemb,* 2017; **45**(1), 14-22

17. Fattahi H. Risk assessment and prediction of safety factor for circular failure slope using rock engineering systems. *Env Earth Sci,* 2017; **76**(5), 224

18. Fattahi H. Applying rock engineering systems to evaluate shaft resistance of a pile embedded in rock. *Geotech Geolog Eng,* 2018; **36**, 3269-3279

19. Fattahi H, Moradi A. A new approach for estimation of the rock mass deformation modulus: a rock engineering systems-based model. *Bull Eng Geol Envt* 2018; **77**, 363-374

20. Faramarzi F, Ebrahimi Farsangi M, Mansouri H. An RES-based model for risk assessment and prediction of backbreak in bench blasting. *Rock Mech Rock Eng* 2013; **46**, 877-887

21. Zhou Q, Herrera J, Hidalgo A. Development of a quantitative assessment approach for the coal and gas outbursts in coal mines using rock engineering systems. *Int J Min Reclam Env* 2019; **33**(1), 21-41

22. Fattahi H, Moradi A. Risk assessment and estimation of TBM penetration rate using RES-based model. *Geotech Geolog Eng* 2017; **35**, 365-376

23. Hasanipanah M, Jahed Armaghani D, Monjezi M, Shams S. Risk assessment and prediction of rock fragmentation produced by blasting operation: a rock engineering system. *Envl Earth Sci,* 2016; **75**, 1-12

24. Saffari A, Sereshki F, Ataei M, Ghanbari K. Applying rock engineering systems (RES) approach to evaluate and classify the coal spontaneous combustion potential in Eastern Alborz coal mines. *Int J Min GeoEng,* 2013; **47**(2), 115-127

25. Azadmehr A, Jalali SME, Pourrahimian Y. An application of rock engineering system for assessment of the rock mass fragmentation: a hybrid approach and case study. *Rock Mech Rock Eng,* 2019; **52**(11), 4403-4419

26. Saeidi O, Azadmehr A, Torabi SR. Development of a rock groutability index based on the Rock Engineering Systems (res): a case study. *Indian Geotech J,* 2014; **44**, 49-58

27. Meten M, Bhandary NP, Yatabe R. Application of GIS-based fuzzy logic and rock engineering system (RES) approaches for landslide susceptibility mapping in Selelkula area of the Lower Jema River Gorge, Central Ethiopia. *Env earth sci,* 2015; **74**, 3395-3416

28. Debnath P, Dey AK. Prediction of bearing capacity of geogrid-reinforced stone columns using support vector regression. *Int Jl Geomech,* 2018; **18**(2), 04017147

29. ASTM: *Standard test method for determining tensile properties of geogrid by single or multi-rib tensile methods. D6637, West Conshohocken, PA* 2001;

30. ASTM: S*tandard practice for classification of soils for engineering purposes (unified soil classification system). D2487, West Conshohocken, PA* 2006;

31. Indian Standard, I: *Design and construction for ground improvement-Guidelines. Part 1: Stone columns. IS* 2003; **15284**, 267-290

32. Han J, Gabr M. Numerical analysis of geosynthetic-reinforced and pile-supported earth platforms over soft soil. *J Geotech Geoenvironmental Eng,* 2002; **128**(1), 44-53

33. Montgomery DC, Peck EA, Vining GG. *Introduction to linear regression analysis*. John Wiley & Sons, (2021)

34. Seber GA, Lee AJ. *Linear regression analysis*, vol. 330. John Wiley & Sons, (2003)

35. Hudson J. *Rock engineering systems*. Theory and practice. (1992)

36. Lu P, Latham J-P. A continuous quantitative coding approach to the interaction matrix in rock engineering systems based on grey systems approaches. *In: International congress International Association of Engineering Geology* 1994, pp. 4761-4770

37. Benardos A, Kaliampakos D. A methodology for assessing geotechnical hazards for TBM tunnelling—illustrated by the Athens Metro, Greece. *Int J Rock Mech Min Sci Geomech Abstr* 2004; **41**(6), 987-999

38. Fattahi H. Indirect estimation of deformation modulus of an in situ rock mass: an ANFIS model based on grid partitioning, fuzzy c-means clustering and subtractive clustering. *Geosci J*, 1-10

39. Fattahi H. Application of improved support vector regression model for prediction of deformation modulus of a rock mass. *Eng Comput* 2016; **32**(4), 567–580

40. Fattahi H. Applying soft computing methods to predict the uniaxial compressive strength of rocks from schmidt hammer rebound values. *Comput Geosci* 2017; **21**(4), 665-681

41. Fattahi H. Tunnel boring machine penetration rate prediction based on relevance vector regression. *Int J Optim Civil Eng,* 2019; **9**(2), 343-353

42. Pourrostam D, Mousavi S, Bakhshpoori T, Shabrang K. Modeling the compressive strength of concrete made with expanded perlite powder. *Int J Optim Civil Eng* 2020; **10**(2), 201-215

43. Kaveh A, Hamze-Ziabari SM, Bakhshpoori T. Estimating drying shrinkage of concrete using a multivariate adaptive regression splines approach. *Int J Optim Civil Eng* 2018; **8**(2), 181-194

44. Kaveh A, Hamze-Ziabari S, Bakhshpoori T. Feasibility of pso-anfis-pso and ga-anfis-ga models in prediction of peak ground acceleration. *Int J Optim Civil Eng,* 2018; **8**(1), 1-14